ACADEMIC PRESS

Available online at www.sciencedirect.com

SCIENCE DIRECT®

Journal of Sound and Vibration 270 (2004) 171–190

JOURNAL OF SOUND AND VIBRATION

www.elsevier.com/locate/jsvi

Axisymmetric wave propagation in fluid-filled pipes: wavenumber measurements in in vacuo and buried pipes

J.M. Muggleton[a,*], M.J. Brennan[a], P.W. Linford[b]

[a] *Institute of Sound & Vibration Research, Southampton University, Highfield, Southampton SO17 1BJ, UK*
[b] *School of Information Systems, University of East Anglia, Norwich, Norfolk NR4 7TJ, UK*

Received 24 September 2002; accepted 8 January 2003

Abstract

Detection of water leaks in buried distribution pipes using acoustic methods is common practice in many countries. Correlation techniques are widely used in leak detection, but for these to be effective, the propagation wave speeds and wave attenuation must be known. Relatively predictable for metal pipes, these are largely unknown for the newer plastic pipes, being highly dependent on the pipe wall properties and the surrounding medium. In a previous paper a theoretical model of a buried fluid-filled pipe to predict both wavespeed and attenuation was presented; the aim of the work in this paper is to validate this model experimentally. Wavenumber measurements, encompassing both wavespeed and wave attenuation are made on a water-filled pipe in vacuo and on a buried water-filled pipe. In general, the measurements show good agreement with the theoretical predictions.

1. Introduction

Detection of water leaks in buried distribution pipes using acoustic methods is common practice in many countries [1,2]. Correlation techniques are generally used to locate the leaks, and although these techniques have been successful for many years when used with metal pipes, they remain problematic when used with plastic pipes [3]. The main reason for this is the effect that the pipe and the surrounding earth have on both the propagation speed of the acoustic wave generated by the leak, and the decay of the wave as it propagates along the pipe. A theoretical model of a buried fluid-filled pipe to predict both wavespeed and attenuation was developed by Muggleton et al. [4]; the aim of the work in this paper is to validate this model experimentally.

*Corresponding author. Tel.: +44-23-8059-2936; fax: 44-23-8059-3190.
E-mail address: jm9@soton.ac.uk (J.M. Muggleton).

0022-460X/03/$ - see front matter
doi:10.1016/S0022-460X(03)00489-9

Acoustic energy in buried water pipes generated by a leak propagates at relatively low frequencies, generally less than 200 Hz, and so it is the low-frequency dynamics of the system, well below the ring frequency of the pipe, that is of interest. At frequencies much less than the pipe ring frequency, four wave types are responsible for most of the energy transfer [5,6]: three axisymmetric waves, $n = 0$, and the $n = 1$ wave, related to beam bending. Of the $n = 0$ waves, the first, termed $s = 1$, is a predominantly fluid-borne wave; the second wave, $s = 2$, is predominantly a compressional wave in the shell; the third wave, $s = 0$, is a torsional wave uncoupled from the fluid. In previous work, wavenumbers were derived for the $s = 1$ and 2 axisymmetric wave types for a fluid-filled elastic pipe both in vacuo [5], and surrounded by an infinite elastic medium [4].

The focus of this work is the experimental determination of the wavenumber of the 'fluid-borne' ($s = 1$) axisymmetric ($n = 0$) wave. Measurements are made on a pipe in vacuo and on a buried pipe. The measurements are compared with theoretical predictions in Ref. [4].

2. Theory

The pipe equations for $n = 0$ axisymmetric wave motion for a fluid-filled pipe, both in vacuo and surrounded by an infinite elastic medium have been derived previously [5,4], and expressions for the wavenumbers for the $s = 1$ and 2 waves have been found. For clarity, these results are reproduced in the following sub-sections.

2.1. The fluid-borne $s = 1$ wave

The wavenumber, k_1, of the axisymmetric ($n = 0$), fluid-dominated ($s = 1$) wave in a buried, fluid-filled pipe is given by [4]

$$k_1^2 = k_f^2\left(1 + \frac{2B_f/a}{Eh/a^2 - \omega^2(\rho h + M_{rad}) + \mathrm{i}\omega R_{rad}}\right), \tag{1}$$

where k_f is the contained fluid wavenumber; ω is the angular frequency; B_f is the bulk modulus of the contained fluid; a and h are the radius and thickness of the shell wall, respectively ($h \ll a$); E is the shell material Young's modulus, which may be complex if the material is lossy ($E \to E(1 + \mathrm{i}\eta)$ where η is the material loss factor); ρ is the density of the shell material; and M_{rad} and R_{rad} are the mass and resistance components of the radiation impedance, z_{rad}, of the surrounding medium at the pipe wall, such that [4,7]

$$z_{rad} = R_{rad} + \mathrm{i}\omega M_{rad} = \sum_m \frac{-\mathrm{i}\rho_m c_m k_m}{k_{m1}^r}\frac{\mathrm{H}_0(k_{m1}^r a)}{\mathrm{H}_0'(k_{m1}^r a)} \tag{2}$$

ρ_m, c_m, and k_m are the density, wavespeed and wavenumber, respectively, of each wavetype present in the surrounding medium, and the summation is performed over all wavetypes present. k_{m1}^r, is the radial component of the wavenumber in the surrounding medium, given by

$$(k_{m1}^r)^2 = k_m^2 - k_1^2. \tag{3}$$

H_0 is a Hankel function of the second kind, representing outgoing waves when the $e^{i\omega t}$ time dependence is adopted, and the prime denotes differentiation with respect to the argument. It is assumed that the surrounding medium is of infinite extent, so that no incoming waves are present.

When the argument of the Hankel function is purely (or predominantly) real, it is found that the radiation impedance is complex, with positive real and imaginary components [7,8]. Conversely, when the argument of the Hankel function is purely (or predominantly) imaginary, the resulting radiation impedance is purely (or predominantly) imaginary and mass-like (i.e., positive) [7,8].

Expressing k_1 in the form of Eq. (1) allows the individual terms to be readily identified as stiffness components of the contained fluid ($2B_f/a$) and the pipe wall (Eh/a^2), a pipe wall mass component ($\rho h\omega^2$), and the radiation mass and resistance of the surrounding medium (M_{rad} and R_{rad}). Alternatively, Eq. (1) may be re-expressed in terms of the impedances of the fluid, pipe wall and surrounding medium as

$$k_1^2 = k_f^2\left(1 + \frac{z_{fluid}}{(z_{pipe} + z_{rad})}\right), \tag{4}$$

where $z_{fluid} = -2iB_f/(a\omega)$ and $z_{pipe} = i(\rho h\omega - Eh/(a^2\omega))$.

For the in vacuo case, the radiation impedance term is zero, and the expression for k_1 becomes

$$k_1^2 = k_f^2\left(1 + \frac{z_{fluid}}{z_{pipe}}\right) = k_f^2\left(1 + \frac{2B_f/a}{(Eh/a^2 - \omega^2\rho h)}\right). \tag{5}$$

At low frequencies, this reduces to

$$k_1^2 = k_f^2\left(1 + \frac{2B_f/a}{Eh/a^2}\right), \tag{6}$$

which is recognizable as the non-dispersive Korteweg equation [9].

2.2. The shell-dominated $s = 2$ wave

The wavenumber, k_2, of the axisymmetric ($n = 0$), shell-dominated ($s = 2$) wave in a buried, fluid-filled pipe is given by [4]

$$k_2^2 = k_L^2\left(1 + \frac{\nu^2}{1-\nu^2}\frac{Eh/a^2}{Eh/a^2 + 2B_f/a - \omega^2(\rho h + M_{rad}) + i\omega R_{rad}}\right), \tag{7}$$

where k_L is the wavenumber of a compressional wave in a plate $k_L^2 = \omega^2\,\rho(1-\nu^2)/E$.

Here, M_{rad} and R_{rad} are the mass and resistance components of the $s = 2$ radiation impedance, z_{rad}, defined as [4,7]

$$z_{rad} = R_{rad} + i\omega M_{rad} = \sum_m \frac{-i\rho_m c_m k_m}{k_{ms}^r}\frac{H_0(k_{m2}^r a)}{H_0'(k_{m2}^r a)}. \tag{8}$$

Again, H_0 is a Hankel function of the second kind, representing outgoing waves when the $e^{i\omega t}$ time dependence is adopted, and the prime denotes differentiation with respect to the argument. k_{m2}^r, is the radial component of the wavenumber in the surrounding medium, given by

$$(k_{m2}^r)^2 = k_m^2 - k_2^2. \tag{9}$$

As for the expression for k_1 (Eq. (1)) the individual terms in Eq. (7) can be readily identified as stiffness components of the contained fluid ($2B_f/a$) and the pipe wall (Eh/a^2), a pipe wall mass component ($\rho h\omega^2$), and the radiation mass and resistance of the surrounding medium (M_{rad} and R_{rad}). Alternatively, Eq. (7) may be re-expressed in terms of the impedances of the contained fluid, z_{fluid}, the impedance of the pipe wall, z_{pipe}, the impedance of the pipe wall stiffness, z_{Kpipe}, and the radiation impedance, z_{rad}, viz.,

$$k_2^2 = k_L^2\left(1 + \frac{\nu^2}{(1-\nu^2)}\frac{z_{Kpipe}}{(z_{pipe}+z_{fluid}+z_{rad2})}\right), \tag{10}$$

where $z_{fluid} = -2\mathrm{i}B_f/(a\omega)$, $z_{pipe} = \mathrm{i}(\rho h\omega - Eh/(a^2\omega))$ and $z_{Kpipe} = -\mathrm{i}Eh/(a^2\omega)$.

For the in vacuo case, the radiation impedance term is zero, and the expression for k_2 becomes

$$k_2^2 = k_L^2\left(1 + \frac{\nu^2}{(1-\nu^2)}\frac{Eh/a^2}{(Eh/a^2 + 2B_f/a - \rho h\omega^2)}\right). \tag{11}$$

At low frequencies, this reduces to the non-dispersive form

$$k_2^2 = k_L^2\left(1 + \frac{\nu^2}{(1-\nu^2)}\frac{Eh/a^2}{(Eh/a^2 + 2B_f/a)}\right). \tag{12}$$

3. Measurements on an in vacuo pipe

3.1. Theoretical basis for wavenumber measurements in a finite pipe

In this section, the acoustic wavenumber of axisymmetric waves propagating in a finite pipe (either in vacuo or buried) with unknown termination is determined from pressure measurements made at three separate locations along the pipe. The method is a refinement of that adopted by Prek [10] in which the measurement locations are equally spaced.

Consider a fluid-filled pipe of arbitrary length, as shown in Fig. 1. A plane pressure excitation $p_0\mathrm{e}^{\mathrm{i}\omega t}$ is applied at the end $x = 0$.

The pressure at any point along the pipe, $p(x, t)$, can be represented by two travelling waves, travelling in opposing directions

$$p(x,t) = p^+\mathrm{e}^{\mathrm{i}(\omega t - kx)} + p^-\mathrm{e}^{\mathrm{i}(\omega t + kx)}. \tag{13}$$

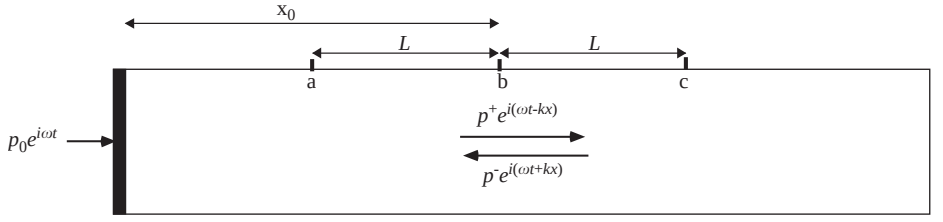

Fig. 1. One-dimensional waves in a finite fluid-filled pipe.

Consider three equispaced locations along the pipe at points a, b, and c, at $x = x_0 - L$, x_0, and $x_0 + L$, respectively, as shown in the figure.

Omitting the time dependence for convenience, the pressures $p(a)$, $p(b)$ and $p(c)$ at the three locations are given by

$$p(a) = p^+ e^{-ik(x_0-L)} + p^- e^{ik(x_0-L)},$$

$$p(b) = p^+ e^{-ikx_0} + p^- e^{ikx_0},$$

$$p(c) = p^+ e^{-ik(x_0+L)} + p^- e^{ik(x_0+L)}. \quad (14a-c)$$

Combining the above three expressions gives an expression for the wavenumber k in terms of the pressures $p(a), p(b)$, and $p(c)$.

Provided that $p(b) \neq 0$,

$$\cos kL = \frac{p(a) + p(c)}{2p(b)} \quad (15)$$

or

$$k = \frac{1}{L} \arccos\left(\frac{p(a) + p(c)}{2p(b)}\right). \quad (16)$$

It should be noted that the wavenumber, k, may be complex and encompasses both the wavespeed and the wave attenuation.

3.2. Experimental set-up and procedure

The experimental arrangement is shown in Figs. 2a and b. It consists of a water-filled MDPE pipe, approximately 2 m in length, secured vertically, with the lower end sealed (Fig. 2a). The

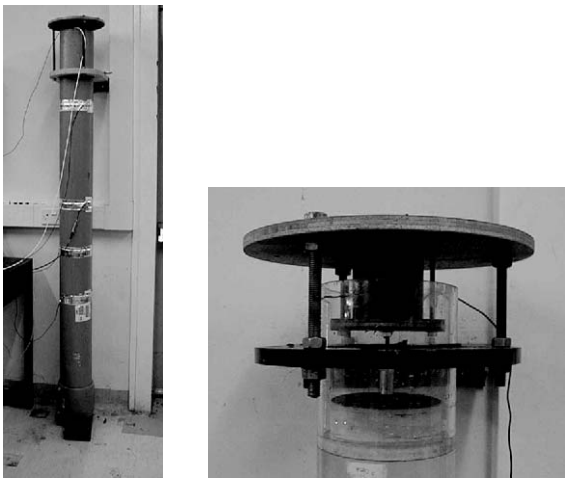

(a) (b)

Fig. 2. (a) Instrumented MDPE pipe. (b) Close-up of exciter and piston (shown here on perspex pipe for clarity).

water column was excited at the upper end by an electrodynamic shaker attached to a light, rigid piston (Fig. 2b). The external diameter of the pipe was 180 mm, with the wall thickness being 11 mm. The centre section of the pipe was instrumented with four calibrated pressure-sensing PVDF wire ring transducers [5], three of which were spaced 0.5 m apart, with the fourth mid-way between the upper two of the three. The piston was excited with a swept sine input from 10 Hz to 1 kHz, and the signals from the transducers subsequently analyzed.

3.3. Experimental results and comparison with theory

The transducer arrangement described above allows for two sets of three equispaced pressure measurements to be analyzed, one set with a 0.25 m spacing, and the second set at 0.5 m spacing.

The experimentally determined wavenumber was calculated using Eq. (16) from each of the two sets of three transducer measurements. The predicted wavenumber was calculated using Eq. (5) and previously measured values of the pipe material and geometrical properties (shown in Table 1). The real and the imaginary components of the measured and predicted wavenumbers are shown in Figs. 3a and b. The imaginary part is expressed as wave attenuation in dB/m where

$$Loss(\mathrm{dB/m}) = \frac{20\,\mathrm{Im}\{k\}}{\ln(10)}.$$

Fig. 3a shows that there is good agreement between the measured and predicted values for the real part of the wavenumber, particularly at low frequencies. The deterioration of agreement with increasing frequency is as expected given that both the measurements and predictions are only valid well below the ring frequency [5] ($\sim$2 kHz for the MDPE pipe). The data for the more closely spaced set is slightly noisier than for the widely spaced transducers, the differences being greater at low frequencies. This again is as expected, given that discrimination for the longer wavelengths will be improved with more widely spaced transducers, particularly near pressure antinodes. In agreement with the predicted data, at low frequencies, the wavenumber varies approximately linearly with frequency, implying a frequency-independent wavespeed. From the figure, this wavespeed can be deduced to be around 300 m/s.

Fig. 3b shows that the agreement between the measured and predicted data for the imaginary part of the wavenumber is less good than for the real part. The mean values for the measured data show good agreement, particularly at low frequencies, but the deviations from the mean are larger. Again, the data from the more widely spaced transducers are superior. The figure shows

Table 1
Geometrical and material properties of MDPE pipe (figure in parentheses indicates low-temperature measurement)

Mean radius (m)	84.5×10^{-3}
Wall thickness (m)	11×10^{-3}
Density (kg/m^3)	900
Young's Modulus (GN/m^2)	1.6 (2.0)
Loss factor	0.06

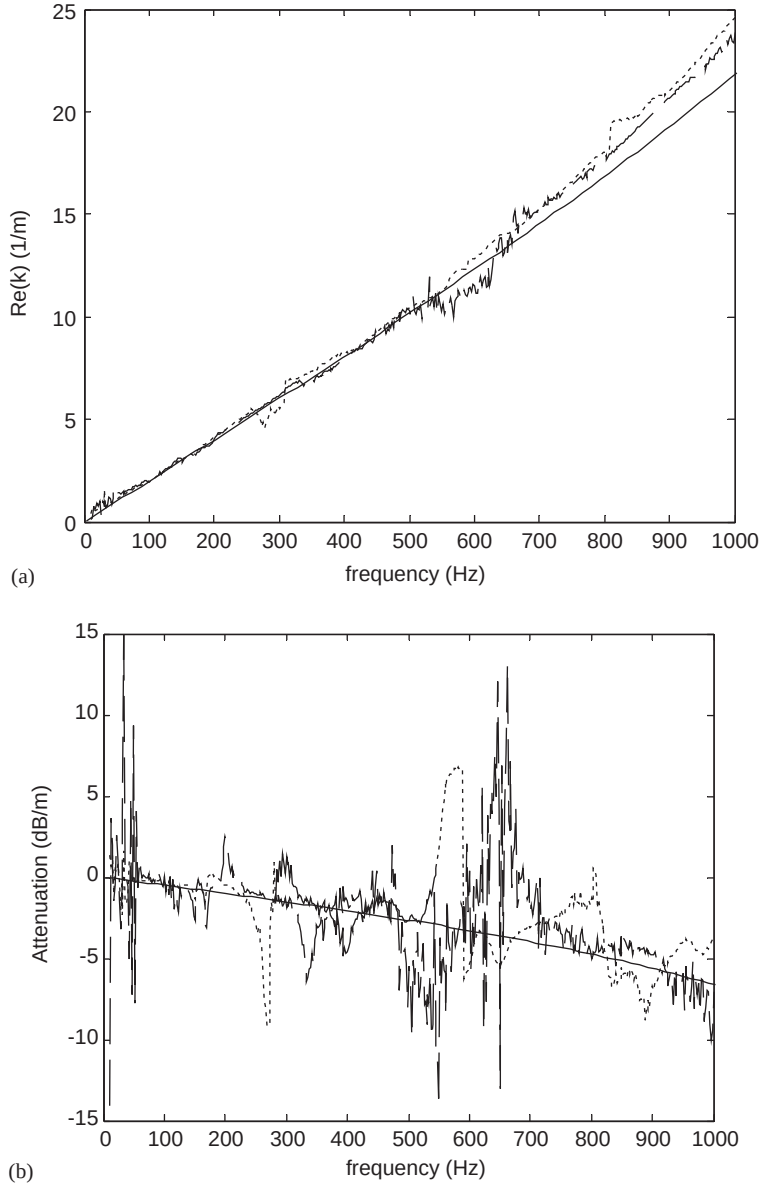

Fig. 3. Wavenumber for the axisymmetric 'fluid-borne' wave: (a) real part; (b) imaginary part; —— predicted ; ..... measured (0.5 m spacing); - - - - - measured (0.25 m spacing).

that, at 400 Hz for example, the wave attenuation is around 2 dB/m, indicating that, in the absence of reflected waves, the pressure would halve approximately every 3 m. This attenuation is due to losses within the shell wall, as the wall inflates and deflates in response to the internal fluid pressure.

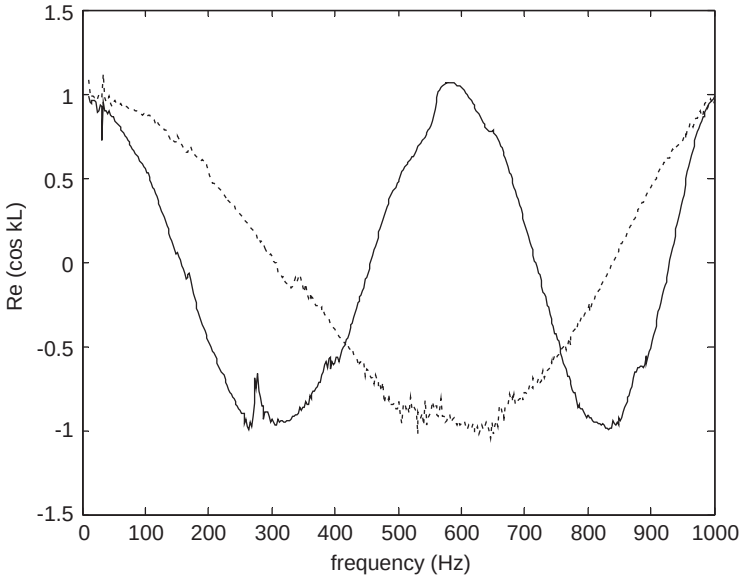

Fig. 4. $\mathrm{Re}\{\cos kL\}$ vs. frequency: —— 0.5 m spacing; ..... 0.25 m spacing.

Returning to the two sets of measured data, one disadvantage to the more widely spaced transducers is associated with "unwrapping" of the data. Once there is more than half a wavelength between adjacent transducers, the data must be "unwrapped" when the arccos of the pressure ratios is calculated (Eq. (16)).

$$\mathrm{Re}\{k_{unwrap}\} = \frac{1}{L}((n+1)\pi - \mathrm{Re}\{kL_{pv}\}), \quad n \text{ odd},$$

$$\mathrm{Re}\{k_{unwrap}\} = \frac{1}{L}(n\pi + \mathrm{Re}\{kL_{pv}\}), \quad n \text{ even},$$

$$\mathrm{Im}\{k_{unwrap}\} = \frac{1}{L}(-1)^n \mathrm{Im}\{kL_{pv}\}, \qquad (17\mathrm{a}-\mathrm{c})$$

where kL_{pv} is calculated from the principal value of the arccos, and n is the number of half wavelengths between adjacent transducers.

Fig. 4 shows measured values of $\mathrm{Re}\{\cos kL\}$ plotted against frequency for both sets of data. Fig. 5 shows the pre- and post-unwrapped data for the real part of the wavenumber for the 0.5 m spaced transducers.

Clearly, the further apart the transducers are spaced, the more "unwrapping" will need to be done, and a balance must be achieved between the improved discrimination achieved with widely spaced transducers, and the number of half wavelengths occurring between them at the maximum frequency of interest.

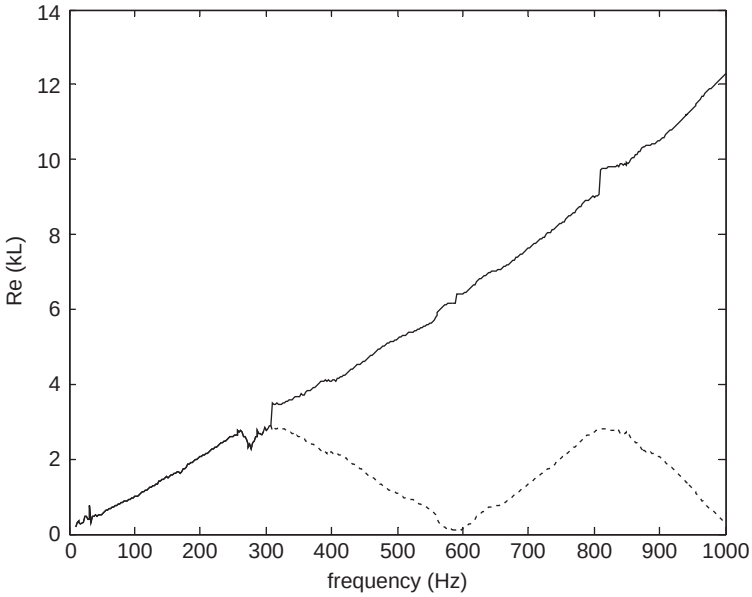

Fig. 5. Re$\{kL\}$ vs. frequency: ——, pre-unwrapping; - - - - -, post-unwrapping.

4. Measurements on a buried pipe

4.1. Experimental rig and data acquisition

To make measurements on a buried pipe, a facility already available at the University of East Anglia was used. This rig was originally designed to allow sounders and sensors to be tested and developed in an acoustically quiet environment operating at a low pressure. It was not intended to be an accurate simulation of an in-service main since the pipe in the rig is not pressurized (apart from the approximately 1.5 m standing head) and there is no flow. Fig. 6a shows a schematic of the test rig.

The pipe in the test rig is 180 mm MDPE comprising a number of 4 m lengths and T-sections, with the 4 m lengths being butt welded and the T-sections being jointed with electro-fusion fittings. A flanged pipe fitting is used to take the pipe through the tank wall. The rig, from tank to tank appears as: 4 m length - T (with a hydrant) - 4 m length - 4 m length - T (with a rotated gate valve) - 4 m length - 4 m length - T (with a rotated gate valve) - 4 m length. Each of the 4 m lengths, and the hydrant T-section, are fitted with two hydrophones which are installed through the pipe wall such that the active face of the sensor is flush with the inside bore of the pipe. The hydrophones, which have a flat frequency response from 1 Hz to approximately 2 kHz, are positioned to give an approximately uniform spacing along the pipe, the exact positions being given in Table 2. The signals immediately pass through an analogue to digital converter (ADC) and the digital stream is returned to the surface using a 20 m cable. All the cables are gathered together in an equipment hut located half-way along the rig's length. The pipe is terminated at each end in a large tank of approximately 12 cubic metres. Together with the tanks, the rig is

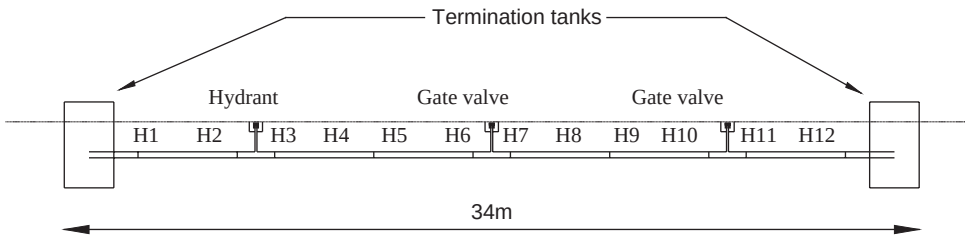

(a)

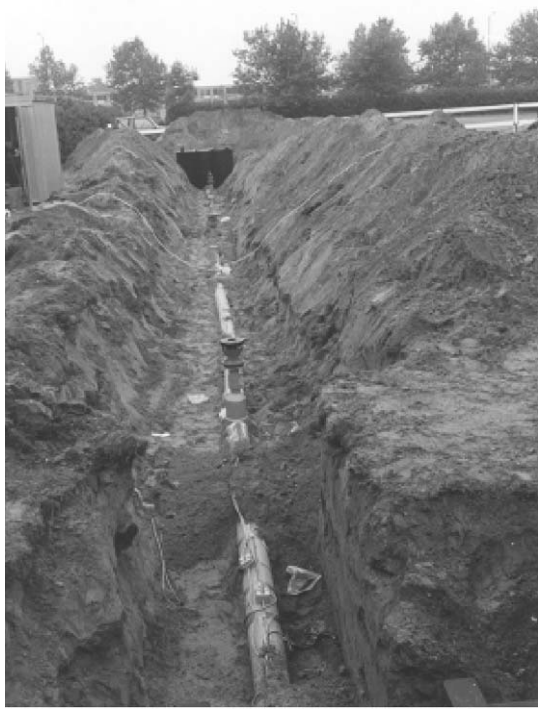

(b)

Fig. 6. (a) The test rig at UEA. (b) The UEA test rig under construction.

approximately 34 m long with the pipe being laid in the standard manner in a mostly sand backfill. Fig. 6b shows the rig under construction where the sensors and ADC units can be seen as small grey boxes dotted along the length of the pipe. To reduce reflections in the tanks an ''anechoic'' terminator was fitted to the pipe. This takes the form of a pipe section approximately one metre in length that has progressively larger holes drilled in the walls, increasing in size towards the end.

The sounder used for the work presented in this paper, is a modified moving-coil underwater loudspeaker. It has been back-filled with concrete to provide a reaction mass and is mounted in a standard 180 mm flanged pipe fitting. Two views of this sounder design are shown in Fig. 7. The

Table 2
Hydrophone positions and maximum frequencies for valid data

Hydrophone	Distance from sounder (m)	Maximum frequency for valid data (Hz)
H1	2.00	> 750
H2	4.02	750
H3	7.43	450
H4	9.45	350
H5	11.39	380
H6	13.44	400
H7	16.77	310
H8	18.80	300
H9	20.76	275
H10	22.80	175
H11	26.25	—
H12	28.28	—

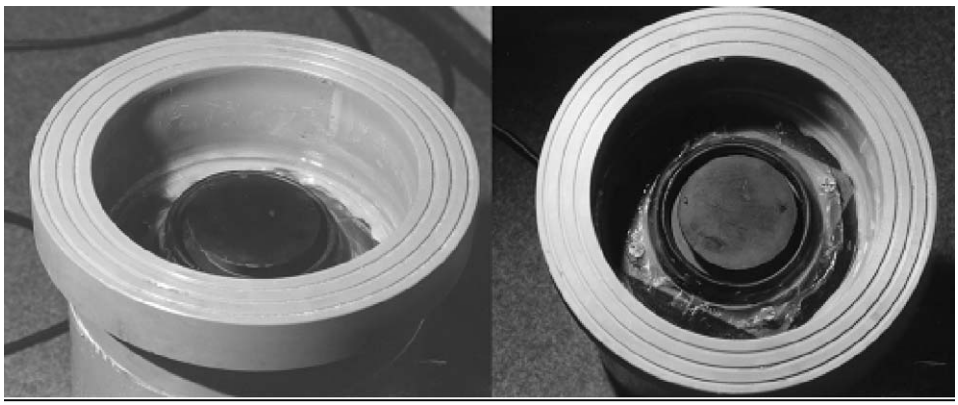

Fig. 7. The pipe sounder.

use of this sounder limits the lowest frequency at which measurements can be made to approximately 30 Hz.

For these tests, the sounder was excited with a stepped sine input from 30 Hz to 1 kHz at 1 Hz intervals. Signals were acquired from each of the hydrophones, referenced to the signal from the hydrophone closest to the sounder, H1. The signals were then analyzed as described in the following sub-sections.

4.2. Analysis procedure

Preliminary tests on the rig indicated that the pipe could be considered anechoic for the fluid dominated ($s = 1$) wave at all the frequencies of interest. As mentioned in the previous sub-section, the pipe was fitted with a termination intended to be anechoic, but in addition, the pipe length was sufficient for the highly attenuated $s = 1$ wave to be virtually undetectable at the far end of the pipe. These tests also revealed the maximum frequency at which data from each

hydrophone could be considered valid (i.e., above the 'noise floor'). These maximum frequencies are shown in Table 2.

For the case of no returning wave, Eq. (14) becomes

$$p(a) = p^{+}\mathrm{e}^{-\mathrm{i}k(x_0-L)},$$

$$p(b) = p^{+}\mathrm{e}^{-\mathrm{i}kx_0},$$

$$p(c) = p^{+}\mathrm{e}^{-\mathrm{i}k(x_0+L)}. \tag{18a – c}$$

Under these circumstances it is possible to determine the acoustic wavenumber using only pairs of transducers, for example

$$\mathrm{e}^{-\mathrm{i}kL} = \frac{p(b)}{p(a)}, \tag{19}$$

giving, for complex k

$$\mathrm{Re}\{k\} = -\frac{1}{L}\left(\arg\left(\frac{p(b)}{p(a)}\right) - (n+1)\pi\right), \quad n \text{ odd},$$

$$\mathrm{Re}\{k\} = -\frac{1}{L}\left(\arg\left(\frac{p(b)}{p(a)}\right) - n\pi\right), \quad n \text{ even},$$

$$\mathrm{Im}\{k\} = \frac{1}{L}\ln\left(\left|\frac{p(b)}{p(a)}\right|\right). \tag{20a, b}$$

Again, phase unwrapping for the real part of the wavenumber is required; arg here denotes the value of the phase between $-\pi$ and π, and n is the number of complete half wavelengths between adjacent transducers.

4.3. Experimental results and comparison with theory

The transducer layout described in Section 4.1 allows for a number of pairs of pressure measurements to be analyzed. However, given the rapid decay of the acoustic pressure with distance along the pipe, the baseline data was derived from the first pair of hydrophones (H1 and H2, Table 2). Subsequent hydrophones were then used to investigate particular aspects of the rig behaviour as discussed below.

The experimentally determined wavenumber was calculated using Eq. (20) applied to the first hydrophone pair. Figs. 8a and b show the real and imaginary components of the measured wavenumber along with the measured values for the in vacuo pipe (shown previously in Fig. 3). Fig. 8a shows that the real part of the wavenumber increases with frequency until around 750 Hz until it starts to drop off, with the 'noise floor' being reached for the farther transducer. Similarly Fig. 8b shows that the magnitude of the imaginary part increases with frequency until around 700 Hz, when the signals begin to drop off. Both the real and imaginary components of the measured wavenumber display fluctuations at low frequencies (below $\sim$150 Hz). Although preliminary tests on the rig indicated that the pipe could be considered anechoic for the fluid dominated wave it is likely that some reflections occurred from the T-section nearest the sounder; the presence of these reflections were thought to be the cause of the observed fluctuations.

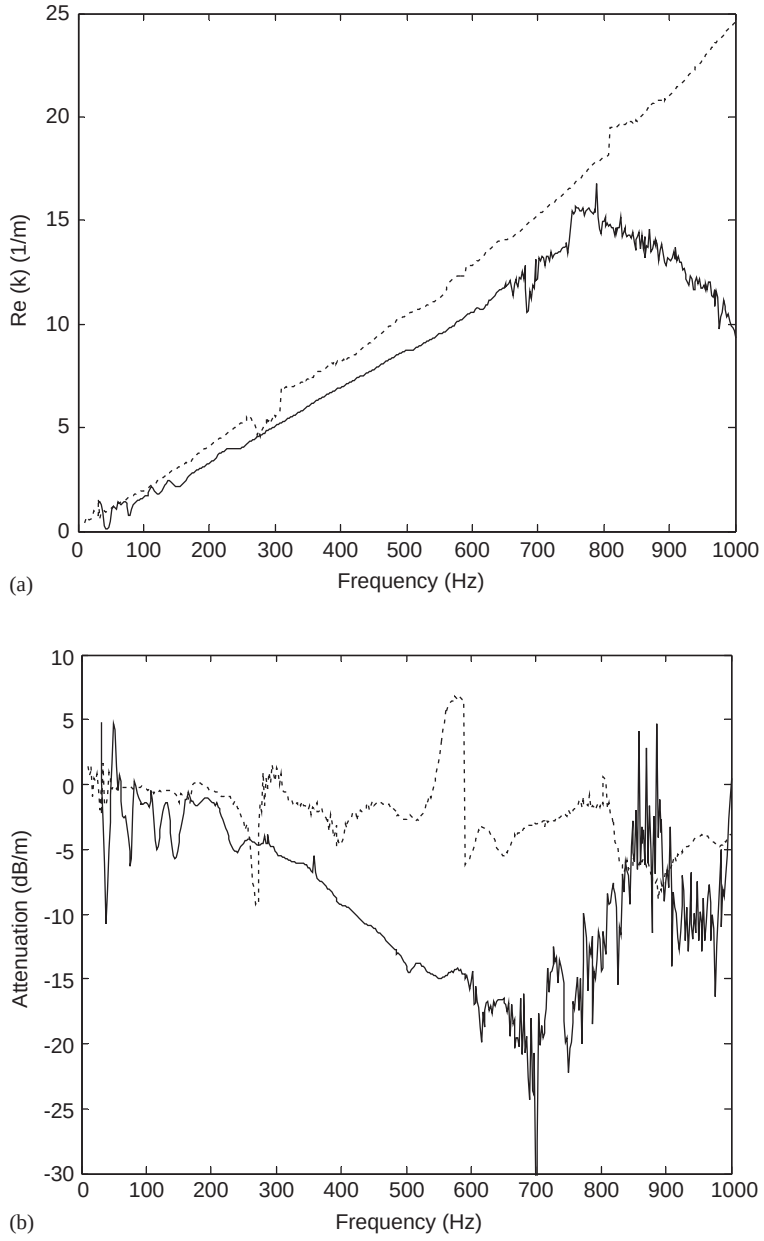

Fig. 8. Measured wavenumber for the axisymmetric 'fluid-borne' wave: (a) real part; (b) imaginary part; ——, buried pipe; ....., in vacuo pipe (0.5 m spacing).

Comparison with the in vacuo data shows that both the measured attenuation and wavespeed are greater for the buried pipe. That the attenuation is greater ($\sim$10 dB/m compared with $\sim$2 dB/m at 400 Hz) is as expected, given that some radiation into the surrounding ground is anticipated [4,11]. However, the increase in wavespeed (to around 350–400 m/s compared with

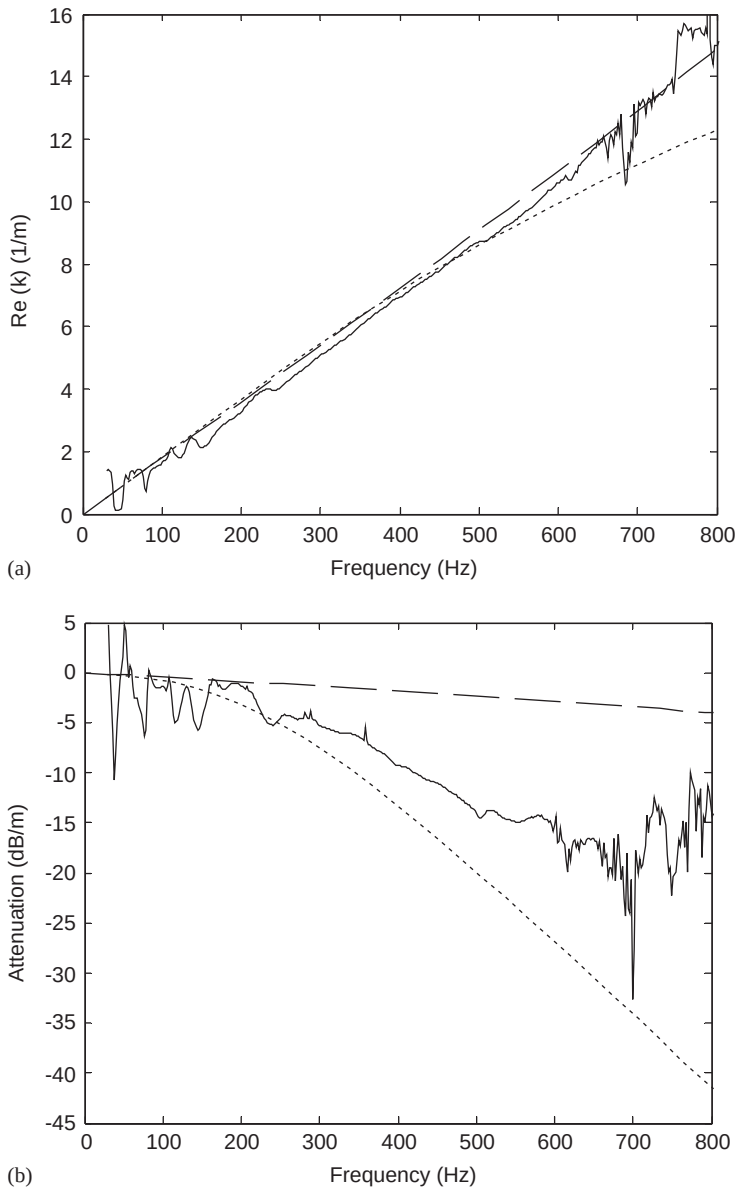

Fig. 9. Measured and predicted wavenumber for the axisymmetric 'fluid-borne' wave in buried pipe: (a) real part; (b) imaginary part; ——, measured; ....., predicted (buried pipe); - - - - -, predicted (in vacuo pipe).

300 m/s) is a surprise at first sight. The effect (however small) of the surrounding medium, at low frequencies, will be to mass load the pipe so a decrease in wavespeed, even if only a small one under certain circumstances, would be expected [4,11]. The increase in wavespeed must be due to an increase in stiffness, and this is most likely to be in the pipe wall itself. The elastic properties of MDPE vary with temperature, the temperature in the ground being only a few °C at the time of making the measurements, compared with around 20°C in the laboratory.

Table 3
Material properties of loose unsaturated sand [12]

Density (kg/m^3)	1500
Longitudinal wavespeed (m/s)	200
Shear wavespeed (m/s)	100

The real and the imaginary components of the measured and predicted wavenumbers are shown in Figs. 9a and b for the buried pipe. The predicted wavenumber was calculated using Eq. (1) using measured values of the pipe material properties at low temperatures, along with typical wavespeed and density data for loose unsaturated sand (a good representation of the soil in which the pipe was buried), shown in Table 3 taken from Ref. [12]. Also shown is a low-temperature prediction for an in vacuo pipe.

Fig. 9a shows that there is good agreement between the measured and predicted values for the real part of the wavenumber, particularly at low frequencies (up to around 500 Hz). Above this frequency, the measured wavenumber seems to match the in vacuo prediction better than the buried pipe prediction, which starts to fall off above 500 Hz. Soil properties can be extremely variable and are notoriously difficult to determine, and it was found that in this slightly higher frequency region, the prediction was sensitive to the properties chosen. Furthermore, the reason for the fall-off in the buried pipe prediction is not entirely clear at present, and is the subject of current investigation.

Fig. 9b shows that the marked increase in attenuation predicted for the buried pipe compared with the in vacuo case is borne out in practice. There is fair agreement between the measured and predicted values for the imaginary part of the wavenumber, with the trend of increasing attenuation with frequency being reproduced, but with the measured wave attenuation being somewhat less than the predicted attenuation. Apart from the uncertainty of the soil properties, this could, in part, be due to the $s = 1$ wave being energized by the $s = 2$ wave as it propagates (at pipe discontinuities, for example). In making the measurements it has been assumed that by exciting only the fluid, only the $s = 1$ wave will be excited. This is not, in fact, the case. As the fluid and structural waves are coupled, even pure pressure excitation in the fluid will, to a small degree, excite the shell-dominated, $s = 2$ wave. For the MDPE pipe used in the experiments, for pure pressure excitation, the ratio of pressures at the excitation point (attributable to the $s = 1$ wave compared with the $s = 2$ wave) is found to be approximately 100 (see Appendix A for further details). In the absence of wave attenuation this ratio would be maintained along the length of the pipe, suggesting that the contribution from the $s = 2$ wave is negligible. However, both waves attenuate as they propagate. Fig. 9a shows that the $s = 1$ wave is expected to attenuate at approximately 8 dB/m at 300 Hz. Fig. 10 depicts the real and imaginary components of the shell dominated $s = 2$ wave as predicted by Eq. (10) for the buried pipe. The material and geometrical properties used are those given in Tables 1 and 3 with the low-temperature elastic modulus being used. From Fig. 10b it can be seen that the $s = 2$ wave is expected to attenuate at $\sim$0.3 dB/m at 300 Hz. With an initial pressure ratio of around 100, one might then expect the $s = 2$ wave to dominate the signal after approximately 5 m. Fig. 11 shows the real part of the measured wavenumber for the buried pipe derived from four different hydrophone pairs along the pipe. The figure shows that the measured wavenumber is independent of the measurement location along

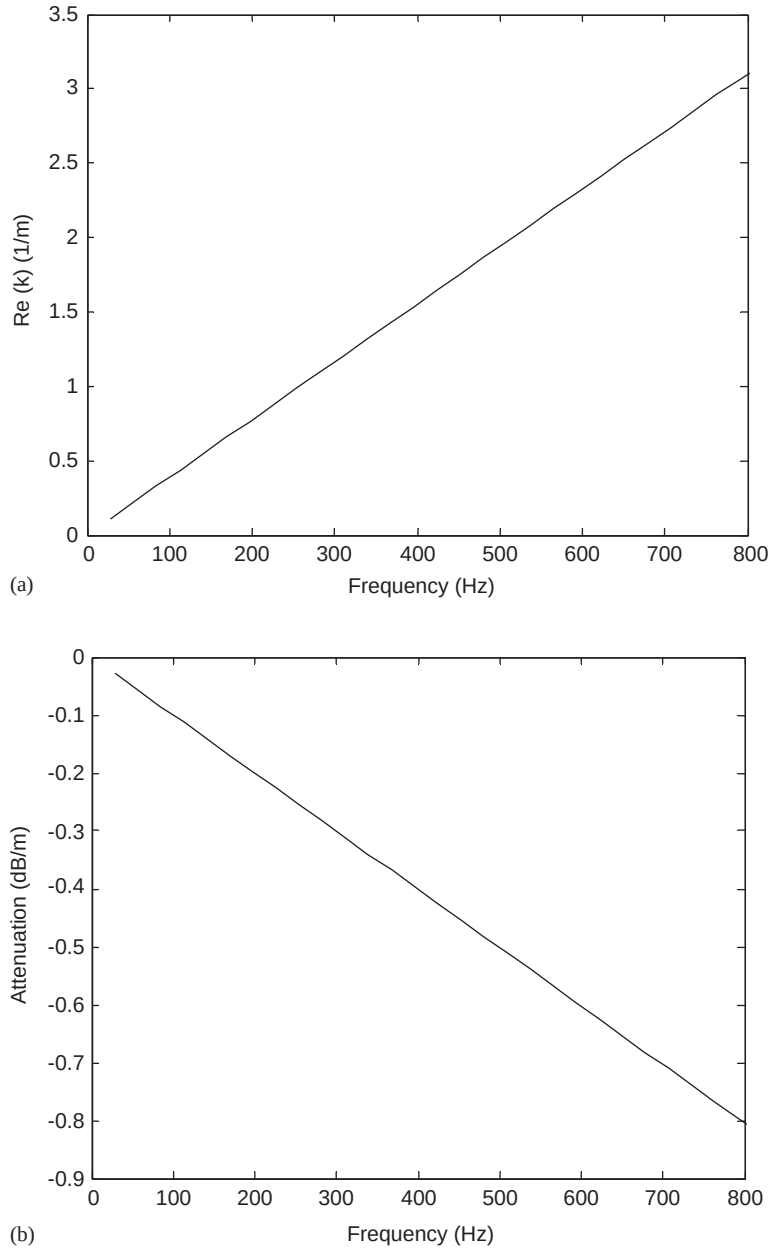

Fig. 10. Measured and predicted wavenumber for the axisymmetric shell dominated wave in buried pipe: (a) real part; (b) imaginary part.

the pipe (accounting for the fact that the signal degrades for the more distant hydrophones), i.e., the wavespeed does not change as the wave propagates along the pipe. This suggests that even at distances of 18 m (the distance of the fourth pair of hydrophones), the $s = 2$ wave is not dominating the signal (Fig. 10a shows that the wavespeed of the $s = 2$ wave is substantially faster

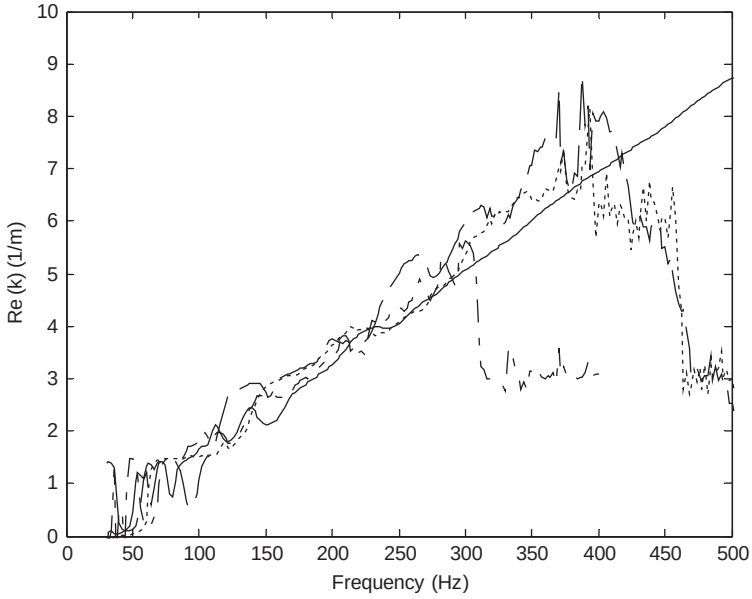

Fig. 11. Measured wavenumber from 4 different hydrophone pairs: ——, H2/H1; ....., H4/H3; - - - - -, H6/H5; -·-·-, H8/H7.

than that of the $s = 1$ wave $-\sim 1600$ m/s compared with ~ 350 m/s). It seems likely that discontinuities along the pipe (for example, the T-sections, welds between pipe lengths, possibly unevenness in the soil surrounding the pipe) cause additional coupling between the wavetypes, enabling the $s = 2$ wave to re-energize the $s = 1$ wave. Appendix A shows that if the coupling was such that there was equal energy in each mode, the pressure attributable to the $s = 2$ wave would be around 1/5 of that attributable to the $s = 1$ wave. It is unlikely that this is the case, as such a large contribution would affect the measured phase, but some additional coupling seems probable. Another possible reason for the measured attenuation being not as expected is the proximity of the ground surface. The model assumes that the pipe is surrounded by an infinite elastic medium. Clearly the ground around the pipe is not infinite, with the surface being approximately 2 m above the pipe. The presence of this free surface will cause reflections of the radiated waves so that the radiation impedance will not be as predicted. It is planned to incorporate a free surface into the model in the near future.

5. Conclusions

In this paper, wavenumber measurements have been made on an in vacuo, and a buried water-filled plastic pipe. Excitation was applied directly in the fluid at frequencies well below the pipe ring frequencies, so the dominant wavetype present was the axisymmetric ($n = 0$), fluid-dominated ($s = 1$) wave. Complex wavenumbers were determined, which encompass both the wavespeed and the wave attenuation.

A novel three-transducer method was used to decompose the waves in the in vacuo pipe, which was not terminated anechoically; a two transducer formulation was found to be sufficient for the buried pipe case due to the much larger wave attenuation.

The measured wavenumbers were then compared with predictions from in vacuo and buried pipe models developed previously. For the in vacuo pipe, the wavespeed was found to compare well with that predicted by the model. The measured attenuation was found to fluctuate, but the average value compared well with the prediction. For the buried pipe, there was good agreement between the measured and predicted wavespeeds, again, particularly at low frequencies; at higher frequencies, the measured wavespeed matched the in vacuo prediction slightly better than the buried pipe prediction, possibly due to uncertainties in the soil properties. The model predicted a marked increased in the wave attenuation compared with the in vacuo case, which was borne out in practice. The measured attenuation, however, was found to be somewhat less than that which was predicted. This was thought to be possibly due to a combination of the influence of the $s = 2$ (shell dominated) wave, uncertainty in the soil properties, and the effect of the ground surface, which was not accounted for in the theoretical modelling.

With regard to acoustic leak detection in plastic pipes, two significant conclusions may be drawn. Whilst the soil surrounding the pipe has been found to have little direct effect on the wavespeed of the 'fluid-borne' wave compared with the in vacuo case, the fact that the elastic properties of the pipe wall are temperature dependent means that it may vary considerably depending on the pipe's environment. If this is not taken into account in calculating the expected wavespeed, leak location errors are liable to be large. The finding that the surrounding soil markedly increases the wave attenuation compared with the in vacuo case suggests an additional difficulty, in that the signal to noise ratio will be substantially reduced.

Acknowledgements

The EPSRC are gratefully acknowledged for their support of this work.

Appendix A. Effects of the $s = 2$ shell-dominated wave

For an elastic pipe, the $s = 1$ (fluid-dominated) and $s = 2$ (shell-dominated) waves both involve motion of the fluid and the shell wall [5]. Thus, even for pure fluid excitation, both modes are excited, and the resulting acoustic pressure in the pipe arises from a combination of the two wave types. In this appendix, the ratio of the pressures associated with these waves is derived for two situations: a pressure pulsation; and equipartition of energy between these waves.

For pressure pulsations, the ratio of radial wall motions $|W_2/W_1|$ associated with the $s = 1$ and $s = 2$ waves, well below the ring frequency, is given by [5]

$$\left|\frac{W_2}{W_1}\right| \approx \left(\frac{k_2}{k_1}\right)^2 \frac{\nu^2}{(1 + (2Ba/Eh)(1 - \nu^2))}. \tag{A.1}$$

This gives the ratio of fluid pressures $|P_2/P_1|$ associated with the $s = 1$ and 2 waves as

$$\left|\frac{P_2}{P_1}\right| \approx \left(\frac{k_2}{k_1}\right)^2 \frac{v^2}{(1-v^2)} \frac{(2Ba/Eh)(1-v^2)}{(1+(2Ba/Eh)(1-v^2))}, \tag{A.2}$$

which, for a soft-walled pipe, can be further approximated as

$$\left|\frac{P_2}{P_1}\right| \approx v^2 \left(\frac{k_2}{k_1}\right)^2. \tag{A.3}$$

If equipartition of energy between the two wave types is assumed, the ratio of radial wall motions, $|W_2/W_1|$, is found to be given approximately by [5]

$$\left|\frac{W_2}{W_1}\right|^2 \approx \left(\frac{k_2}{k_1}\right) \frac{v^2}{((2Ba/Eh)(1-v^2)(1+(2Ba/Eh)(1-v^2)))}. \tag{A.4}$$

This leads to

$$\left|\frac{P_2}{P_1}\right|^2 \approx \left(\frac{k_2}{k_1}\right) \frac{v^2(2Ba/Eh)(1-v^2)}{(1+(2Ba/Eh)(1-v^2))}, \tag{A.5}$$

which for a soft-walled pipe can be further approximated by

$$\left|\frac{P_2}{P_1}\right| \approx v\sqrt{\frac{k_2}{k_1}}. \tag{A.6}$$

Expressions for the wavenumbers of the $s = 1$ and 2 waves in vacuo, are given in Eqs. (6) and (12), respectively.

It can be seen that, at low frequencies, the $s = 1$ and 2 wavenumbers vary linearly with frequency, i.e., the waves are non-dispersive and have a frequency-independent wavespeed. As a result, the pressure ratios defined in Eqs. (A.3) and (A.6) will be frequency-invariant. Substitution of the pipe material properties (Table 1) results in

$$\frac{P_2}{P_1} = O(0.01) \quad \text{for pure pressure excitation,}$$

and

$$\frac{P_2}{P_1} = O(0.2) \quad \text{for well coupled fluid and shell waves.}$$

References

[1] H.V. Fuchs, R. Riehle, Ten years of experience with leak detection by acoustic signal analysis, *Applied Acoustics* 33 (1991) 1–19.

[2] O. Hunaidi, W.T. Chu, Acoustical characteristics of leak signals in water distribution pipes, *Applied Acoustics* 58 (1999) 235–254.

[3] O. Hunaidi, W.T. Chu, A. Wang, W. Guan, Detecting leaks in plastic water distribution pipes, *Journal of the American Water Works Association* 92 (2) (2000) 82–94.

[4] J.M. Muggleton, M.J. Brennan, R.J. Pinnington, Wavenumber prediction of waves in buried pipes for water leak detection, *Journal of Sound and Vibration* 249 (5) (2002) 939–954.

[5] R.J. Pinnington, A.R. Briscoe, Externally applied sensor for axisymmetric waves in a fluid filled pipe, *Journal of Sound and Vibration* 173 (1994) 503–516; doi:10.1006/jsvi.1994.1243.
[6] C.R. Fuller, F.J. Fahy, Characteristics of wave propagation and energy distributions in cylindrical elastic shells filled with fluid, *Journal of Sound and Vibration* 81 (1982) 501–518.
[7] M.C. Junger, D. Feit, *Sound, Structures, and their Interaction*, MIT Press, Cambridge, MA, 1986.
[8] M.C. Junger, The physical interpretation of the expression for an outgoing wave in cylindrical coordinates, *Journal of the Acoustical Society of America* 25 (1953) 40–47.
[9] D.I. Korteweg, Über die Fortpflanzungsgeschwindigkeit des Schalles in elastischen Röhren (On the speed of sound in water in flexible pipes), *Annalen der Physik und Chemie* 5 (1878) 525–542.
[10] M. Prek, Experimental determination of the speed of sound in viscoelastic pipes, *International Journal of Acoustics and Vibration* 5 (3) (2000) 146–150.
[11] J.M. Muggleton, M.J. Brennan, Axisymmetric wave propagation in buried, fluid-filled pipes: effects of the surrounding medium, *Proceedings IOA Spring Conference*, Salford, 25–27 March 2002.
[12] J.M. Head, F.M. Jardine, Ground borne vibrations arising from piling, CIRIA Technical Note 142, 1992.